

Particle transport phenomena in low temperature solids

(Review Article)

M. Bargheer and N. Schwentner

Institut für Experimentalphysik, Freie Universität Berlin
Arnimallee 14, 14195 Berlin, Germany
E-mail: nikolaus.schwentner@physik.fu-berlin.de

Received November 11, 2002

We review different approaches to measure the transport of F atoms and ions in rare gas matrices and compare the experimental results to simulations. Static measurements on sandwich structures and co-doped matrices yield rather long travel ranges beyond 2 nm, in accord with early classical simulations which predict a channeling of the F atoms in rare gas matrices. Nonadiabatic simulations show a rapid energy loss, fast nonadiabatic dynamics and only short travel ranges of typically 1 unit cell. The rapid energy loss, fast nonadiabatic transitions and the timescale for direct dissociation (~ 250 fs) are verified by fs-pump-probe experiments. It remains a challenge to account for the long-range migration when nonadiabatic processes are allowed in simulations, and to measure the long distance flights directly by ultrafast spectroscopy.

PACS: 72.20.Jv

Contents

1. Introduction	225
2. Simulations.	227
3. Escape and transport experiments	228
3.1. Transmission through rare gas overlayers at surfaces.	228
3.2. Sandwich film structures	229
3.3. Multiply doped films and crystals	231
4. Femtosecond pump-probe spectroscopy	231
5. Conclusion	234
Acknowledgment	235
References	235

1. Introduction

The transport of low energy neutral atoms and ions through atomic and molecular layers is of importance in diverse areas such as radiation physics and chemistry, deposition by beams, electrochemistry and chemistry in matrices. This overview tries to tie together theoretical predictions with a set of experimental data from different techniques. It turns out that transport is a significant challenge for the theoretical treatment. Therefore we focus our attention to the transport of small atoms and ions through solid rare gas films, a subject most amenable to theoretical simulations. The interaction of the migrating particles with the rare gas lattice atoms is expected to be strong and from a mechanistic point of view a small particle size should sup-

port migration. The size of an external particle in a lattice is best characterized by the separation of the minimum energy in the pair potential. The pair potentials for a set of neutral atoms with respect to the interaction with Kr atoms, scaled to the Kr–Kr Lennard-Jones potential, are taken from a recent review [1] and displayed in Fig. 1. From the chosen selection it turns out that F atoms have the smallest size of ground state atoms and it may be surprising that even H atoms are considerably larger according to this consideration. Only oxygen atoms in the excited 1D state appear smaller however here we intend to deal only with ground state atoms or ions. Therefore the particles of choice for long range migration are F atoms together with F^+ and F^- ions and we restrict this overview exclusively to those. Information on other particles can

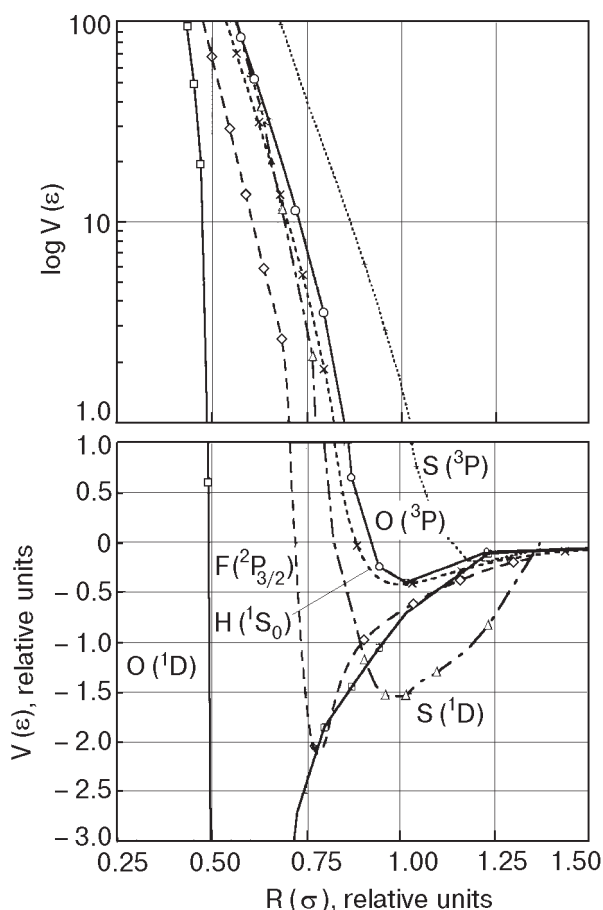


Fig. 1. The sizes of atoms, as discerned from pair potentials with Kr, scaled to the Kr–Kr Lennard-Jones parameters. The lowest energy surface from each of the spin-orbit terms is shown, and the curves are shifted to have a common dissociation limit at zero. The diatomic states corresponding to the various atomic terms are RgX ($^3\Pi$) for X = O(3P) and S(3P), RgX($1^1\Sigma^+$) for X = O(1D), S(1D), and H(1S_0), RgX($I_{1/2}$) for X = F($^2P_{3/2}$). The figure is reproduced from Ref. 1.

be obtained from Ref. 1 and the literature in there. Concerning the term transport, we also intend to restrict ourselves. There is a large body of information on thermally activated migration. The onset of this process at temperatures of 25 K in Ar and 15 K in Kr is shown in Fig. 2 for F atoms. In this article only the migration of «hot» F atoms with kinetic energies well above these thermal energies will be considered. The kinetic energy originates typically from photodissociation of an F containing molecule and the topic of interest is the range of this nonequilibrium particle until it comes to rest due to a sequence of scattering events. Therefore the experiments are carried out in general at temperatures well below the thermal threshold. However, care has to be taken that also unintentional local heating is avoided.

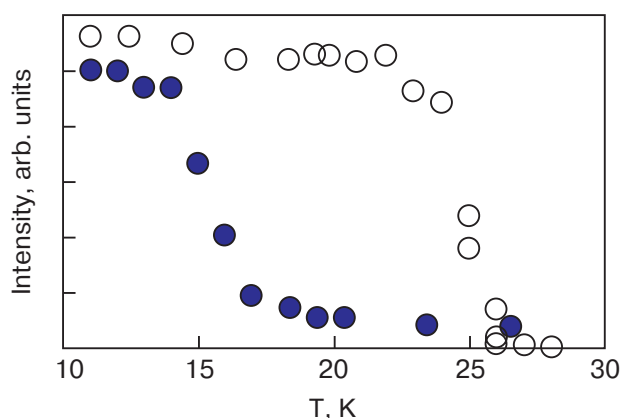


Fig. 2. Fluorescence intensities from RgF excimers after complete dissociation of F₂/Ar 1:4000 (O) and of F₂/Kr 1:3000 (●) by irradiation at 248 nm. The fluorescence is excited with 193 nm in the Ar and 275 nm in the Kr matrix. Heating the samples at a rate of 0.5 K/min yields the thresholds for thermal recombination, indicated by the step in the excimer fluorescence intensity. Figure taken from Ref. 26.

Classical simulations date back to 1984 and they predict a very interesting quite long range motion for F atoms in Ar crystals [2]. Some trajectories showed a motion along «channels» for several lattice constants and one may associate a «channeling» known for energetic particles [3]. The further improvements in theory will be sketched in Sec. 2. The inclusion of nonadiabatic processes and more advanced potential energy surfaces seems to increase in general the interaction with the lattice and to reduce the range. Therefore it remains a challenge to the experiment to separate out a channeling type of motion with a long free path between large angle scattering events in contrast to a diffusive type of motion with a hopping from site to site and without essential angular correlation.

A «Gedanken» experiment using a particle beam well defined in momentum and recording in transmission the change in energy and direction for a variation of the rare gas film thickness monolayer (ML) by monolayer would require a free standing film. The escape experiments described in Sec. 3.1 employ dissociation of molecules positioned well oriented on a single crystalline substrate surface and the penetration of the resulting F ions through the overlaying rare gas films is measured [4]. The transmission of the ions decays to zero already at a rare gas coverage of 1 (2.5) ML for F⁺ (F⁻) ions, indicating a very strong interaction of the ions with the rare gas, while for neutral atoms the detection problem remains unsolved. Therefore, sandwich type of experiments are designed in which F atoms are generated by photodissociation of F₂ in a surface layer. They are sent through a spacer layer with

variable thickness and the penetrating ones are recorded in a substrate layer [5]. The discussion of these experiments in Sec. 3.2 will reveal a moderate penetration depth in Ar of the order of 2 nm or 8 to 9 monolayers. However, the angular information is no longer available. It will be emphasized that assuming a diffusive or channeling type of motion would lead to rather different average length of travel for the same penetration depth.

Another body of information will be considered in Sec. 3.3 in which transport of F fragments between dopants in a rare gas film is studied. Statistical doping is attempted in these experiments which therefore involve averaging on the spatial separation. Rather long ranges of migration are found in several of these experiments. The problem of the spatial averaging and perhaps of multiple excitations which showed up also in the sandwich experiments will be addressed. This type of experiments, however, is essential since it leads into the very heart of chemical applications in the framework of matrix isolation spectroscopy [6,7]. Formation of a high density of F containing compounds can be optimized with these studies. A variety of solid state rare gas excimer lasers with extraordinary high excimer density and thus gain was realized in this way [8,9].

A promising new avenue is presented in Sec. 4 by studying the cage escape of F atoms with femtosecond time resolution [10]. The very first results indicate that it will be possible to follow the F atom migration from site to site. Finally a combination of the time resolved experiment with spatial information proposed in Sec. 5 may lead in the near future to a complete characterization of transport in the spirit of the «Gedanken» experiment.

2. Simulations

In a strictly classical molecular dynamics calculation one F₂ molecule was placed in the center of a cell of 365 Ar atoms with the structure of the fcc lattice [2]. Cage exit probabilities were studied at 4 and 12 K within an excess energy range of 0.5 to 2.8 eV. Inspection of the finally populated sites for 50 trajectories at 12 K showed that 5 F atoms had left the cell. All these trajectories revealed a wiggly motion along a lattice diagonal (110 direction) without sidesteps as demonstrated in Fig. 3. One such trajectory was observed at 2 eV and four at 2.8 eV excess energy. An extrapolation of the path beyond the boundary of the cell according to the calculated small energy loss of 0.5 eV/nm resulted in a total travel length of ~ 3 nm or 12 monolayers. This fascinating long range and channeled motion stimulated further simulations and experimental investigations. The summation of

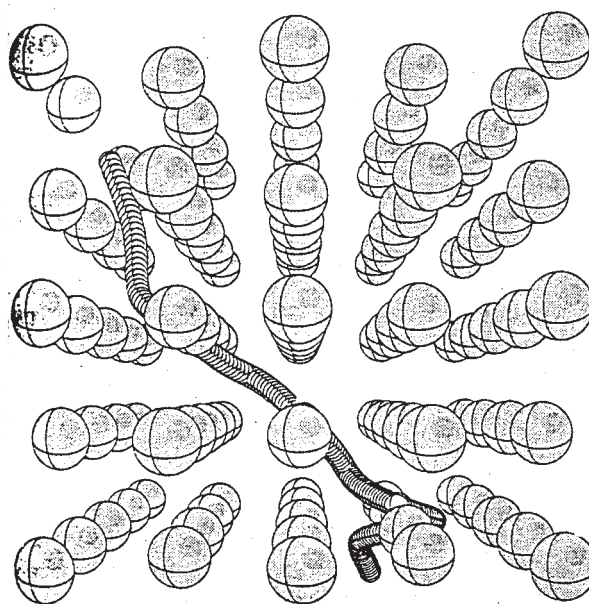


Fig. 3. Result of the earliest classical simulation of an F fragment travelling along the 110 direction after dissociation of F₂ with an excess energy of $E = 2.8$ eV. The sample cell contains 365 Ar atoms at $T = 12$ K and the F fragment finally leaves the cell. Figure taken from Ref. 2.

pair potentials and the relevance of nonadiabatic processes are points of concern, because the interaction of an F(²P_{3/2}) atom with a rare gas atom involves a ground state X_{1/2} and an excited I_{3/2} potential. Running half of the trajectories in a similar slab in Kr on the X_{1/2} and half on the I_{3/2} potential energy surface resulted in a better agreement with the experiment concerning simulated cage exit probabilities versus excess energy than assuming very rapid electronic relaxation to the X_{1/2} surface [11]. Relying still on additive pair potentials and including nonadiabatic processes in a semiclassical way by Tully's surface hopping method showed, however, that reorientation of the *p*-orbitals proceeds very fast in Kr on a time-scale below 100 fs [12,13]. The method was applied to study the migration of F atoms induced by the radiative dissociation after emission of Kr₂⁺F⁻ to the repulsive ground state [13]. The F atoms acquire a kinetic energy of only about 0.2 eV and the heating of the cage due to the Kr–Kr repulsions is included. A significant and fast energy loss by nonadiabatic transitions was observed which substantially shifted the distribution of final distances of the F atoms from the initial position to smaller values. Exclusion of these nonadiabatic contributions resulted in a large probability for cage exit to different sites next to the original F atom position (see Fig. 4) but no F atoms excursions beyond one unit cell were reported. A very instructive statistical treatment of the barrier height distribution from additive pair potentials was applied to F₂ disso-

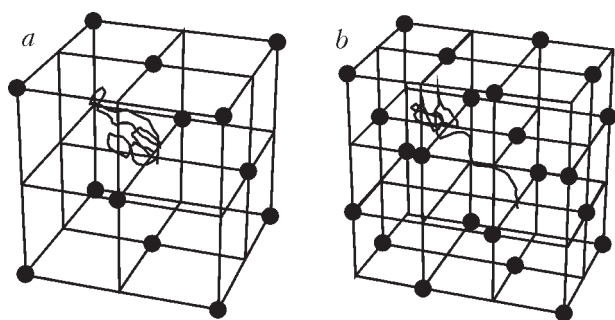


Fig. 4. Two typical adiabatic trajectories for the dissociation of Kr_2F in a Kr matrix. The path of the F atom is shown: *a*) no cage exit, *b*) direct cage exit with stabilization in the O_h interstitial site. The figures are reproduced from Ref. 13, and no trajectories with longer range were reported.

ciation with orbital alignment and cage exit in Ar and Kr [14]. Parallel alignment of the p -hole to the cage wall corresponds to much lower barrier heights. Assuming this favorable orientation yields qualitative agreement with measured cage exit probabilities, however, the simulated absolute values are lower by a factor of two and long range migration was not addressed.

Finally, a major effort was undertaken to go beyond summation of pair potentials and to diagonalize the Hamiltonian for the molecular electronic states in the solid state environment. The potential energy surfaces of 36 electronic states and the nonadiabatic couplings between them were derived from the diatomics-in-molecules approach for F_2 in the center of a

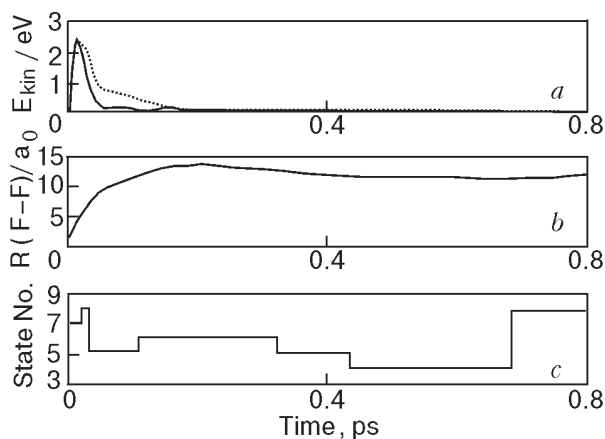


Fig. 5. Direct dissociation of F_2 in an Ar_{54} cluster equilibrated at 8 K and excited with 4.9 eV excess energy. The nonadiabatic calculations demonstrate *a*) rapid energy loss within 0.2 ps, *b*) direct cage exit to the nearest interstitial site at $10 a_0$ and *c*) rapid hopping among the quantum states (numbered from ground state = 1 to the most repulsive valence state = 36) associated with the F_2 molecule. The figures are taken from Ref. 15.

cluster of 54 Ar atoms [15]. Excitation with 4.6 eV and 6.53 eV was considered. All trajectories of the high energy excitation lead to dissociation and direct exit of the cage. The example in Fig. 5 illustrates the fast release of kinetic energy (Fig. 5,*a*) and the manifold of nonadiabatic transitions (Fig. 5,*c*) on a sub-picosecond timescale. The F atom leaves the cage (Fig. 5,*b*) but the F-F amplitude remains between 10 and $15 a_0$ and the F fragments do not leave the cluster itself on the 1–2 ps timescale of the simulations. Thus the question of long range migration is still open. Inclusion of charge transfer contributions by the diatomics-in-ionic-systems method [16], for example, may weaken the interaction strength of the F atom with the lattice. Femtosecond experiments discussed in Sec. 4 allow to follow the fragment motion in real time and provide a more direct way of comparison with the simulations. In essence, it remains to the experiment to settle the contributions of long range trajectories to migration.

3. Escape and transport experiments

3.1. Transmission through rare gas overlayers at surfaces

The transmission of low energy ions through thin films is studied in a long standing effort in relation to the depth of origin of secondary ions. The subject is covered in this volume by the contribution of Madey and a review by Akbulut et al. [17]. Here we include only a brief account on the transmission of F^- and F^+ ions through rare gas films [4] because it is interesting to compare the ion properties with those of neutral atoms. A saturation coverage of PF_3 is condensed on a Ru (0001) surface in a way that it exhibits a $(\sqrt{3} \times \sqrt{3})R30^\circ$ low energy electron diffraction pattern and an azimuthally ordered F^+ and F^- electron stimulated desorption ions angular distribution pattern. Monolayer by monolayer growth of rare gas layers on top of the PF_3 molecules is verified [4]. F^+ , F^- and F_2^- are desorbed by bombardment with 300 eV electrons. The attenuation of the F^+ and the F^- yield with Kr and Xe coverage is displayed in Fig. 6. F^+ ions desorb with a mean kinetic energy of ~ 4 eV and F^- ions have a peak kinetic energy of 0.7 eV. The attenuation for F^+ is very efficient and one monolayer blocks the transmission completely. The effect is attributed to elastic scattering and charge transfer. A small contribution of large angle scattering is in favor of charge transfer contributions. F_2^- attenuation is similarly strong.

The initial increase in F^- yield originates mainly from a suppression of neutralization which occurs near the substrate. Attenuation is once more quite efficient

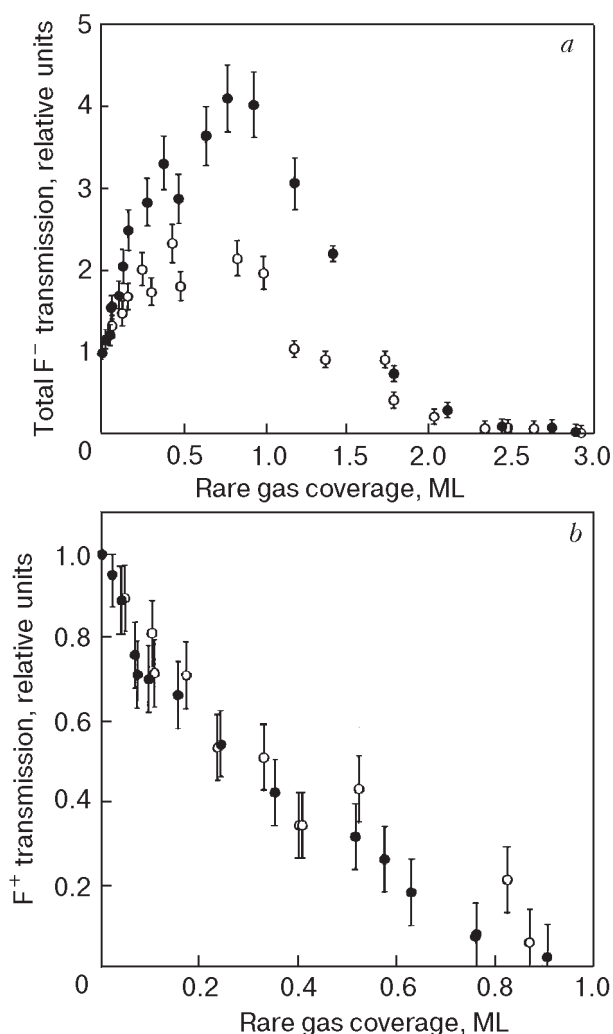


Fig. 6. Plot of the total ion yield generated by electron bombardment of $\text{PF}_3/\text{Ru}(0001)$ as a function of Kr (\circ) and Xe (\bullet) overlayer coverage. The data are normalized to unity for the clean surface value. Figures are reproduced from Ref. 4. *a*) The F^- yield first increases with rare gas coverage, but the transmission decays to zero for 2.5 ML coverage. *b*) The F^+ transmission linearly decays to zero for 1 ML coverage.

and the F^- ions are blocked for film thicknesses between 2 and 2.5 monolayers. Elastic scattering seems to be the dominant attenuation process. The longer range compared to F^+ is attributed to the specific layering in an fcc structure which provides channels perpendicular to the surface until completion of the third layer. The measured angular distribution is in accord with the necessity to direct the escaping F^- ions into the channel direction.

In summary a severe attenuation for the ions is obtained in the escape experiments. However, some type of channeling seems to occur for F^- ions in the thickness regime of 2 monolayers. For a small fraction of O^+ even longer penetration up to 5 or 6 monolayers was observed [18]. Most interesting would be escape

measurements for neutral F atoms which are most likely also present in these experiments. The neutral atoms are more difficult to detect.

3.2. Sandwich film structures

In an alternative approach the transport of neutral F atoms through an Ar spacer layer of variable thickness is studied in a stack of three rare gas films. The inset in Fig. 7 shows a scheme of the sandwich-like structure [19]. 30 to 40 nm of Kr are condensed on a MgF_2 substrate. The thickness of an Ar spacer layer on top of the Kr film is varied from sample to sample between 0 and 100 nm. Finally the structure is closed by an F_2 doped Ar film typically 5 nm thick. The thickness of each layer is carefully controlled by a quartz microbalance. The compactness of the Ar spacer layer is verified by the suppression of surface excitons from the Kr film and the structural quality is optimized by condensation rate and temperature [19]. The F_2 molecules are dissociated using synchrotron radiation with a photon energy of 10.25 eV thus delivering on average a kinetic energy of 4.3 eV to each F atom. The F atoms generated in the top layer which reach the Kr film are recorded by the characteristic Kr_2^+F^- fluorescence. The emission intensity for irradiation during the formation of the stack is displayed in Fig. 7. Besides some background during Kr and Ar condensation, a pronounced increase is observed upon condensation of the F_2/Ar top layer which continues even after completion of the top layer. The increase is attributed to the dissociation of the F_2 content. A frac-

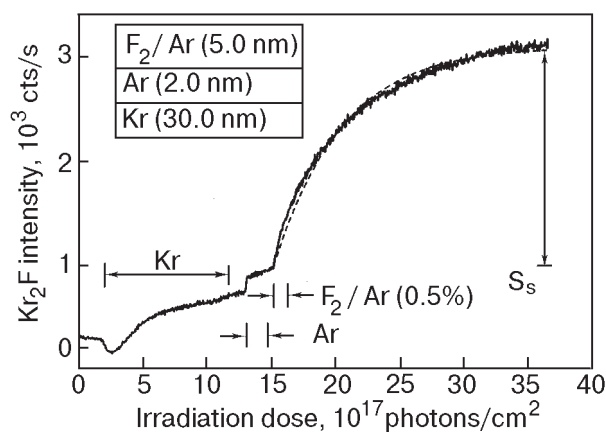


Fig. 7. Intensity dependence of Kr_2F fluorescence at 444 nm for irradiation with 10.15 eV during sandwich condensation. The inset shows the sandwich structure. The background of 1000 cts/s is due to the Kr detection layer and the Ar spacer layer only. Upon condensation of the F_2/Ar (0.5 %) layer, the emission grows and saturates at the signal level S_s . For more detailed discussion see Ref. 19.

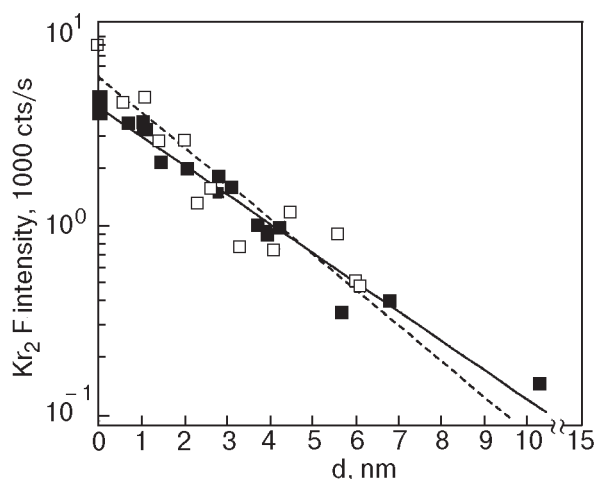


Fig. 8. Saturation value S_s of the Kr_2F fluorescence intensity as a function of the Ar-spacer layer's thickness d for two datasets. The solid and dashed line are exponential fits to the data with decay constants (mean penetration depth) $d_0 = 2.8$ and 2.3 nm, respectively. For a detailed discussion of the experiment see Ref. 19.

tion of the formed F atoms penetrates through the Ar spacer and contributes to the emission. The saturation after prolonged irradiation indicates complete F_2 dissociation and the maximal amount of F atoms which can be kicked by the dissociation process through the spacer layer of Ar. Plotting the saturation values S_s for a set of samples versus the Ar spacer thickness d yields a rather monoexponential decrease of the probability for penetration as shown in Fig. 8. The derived penetration depth d_0 varies between 2.3 and 2.8 nm for two different sets of data indicating a mean penetration for a $1/e$ attenuation of 10 monolayers [19]. Thus a much larger penetration depth is observed for neutral F atoms compared to ions. The value is on the order of magnitude as proposed by the very first classical simulations and it challenges the more advanced calculations. For further consideration one has to distinguish between the penetration depth d_0 measured in this experiment, the average length of travel s_0 and the mean free path l between scattering events. The penetration depth measurement does not directly display, whether the migration is diffusive or predominantly rectilinear due to channeling. In any case, d_0 is a lower limit for s_0 . For a diffusive motion with short l one would obtain a much larger s_0 compared to the measured d_0 . The parallel geometry in the sandwich structure puts also some constraints. For a predominant rectilinear migration with exponential damping, it turns out that only a rather narrow cone of trajectories directed normal to the layers contributes significantly to the signal. The decomposition of d_0 into s_0 and l is not yet unique. A reasonable esti-

mate which is consistent with the measured d_0 yields $s_0 = 7$ nm and $l = 0.9$ nm. Thus for a mean free path l of three monolayers between large energy loss and large angle scattering events one obtains an average length of travel of the order of 7 nm or 28 monolayers. For an extreme diffusive motion with l as small as the nearest neighbor separation an upper limit of $s_0 = 17$ nm is derived.

The detection of the F atoms in the Kr layer is in itself interesting. It is surprisingly efficient. The high sensitivity originates from exciting excitons in the Kr film which transfer their energy to the F atoms [20]. By investigating the dependence of the F emission and Kr emission on the Kr film thickness and by modelling the spectral dependence, it was possible to derive the migration properties of the excitons and the transfer efficiencies. Indeed 10 % of the available light flux can be funneled to a small content of F atoms of only $1/100$ of monolayer by optimizing the experiment. In addition, the Kr emission intensity can be used to normalize the detection efficiency and an improved set of data was obtained with $d_0 = 2.5$ nm [20].

The rise in the signal in Fig. 7 during the deposition of the top layer contains independent information on d_0 . If the F_2 molecules are dissociated efficiently during the layer by layer growth, then those generated later on have to cross the distance between the actual surface and the interface between the Ar/ F_2 film and the Ar spacer film before they enter into the Kr layer. Thus this rise corresponds to a penetration depth measurement with a continuously variable spacer thickness for a single sample [21]. Figure 9 displays the measured rise and its simulation with different d_0 values. Once more, d_0 between 2 and 2.5 nm is obtained.

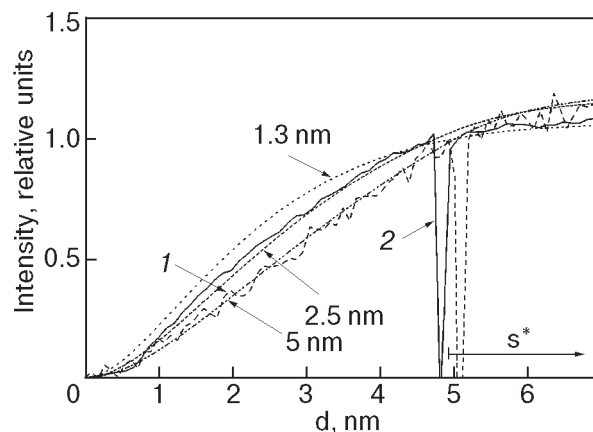


Fig. 9. Normalized measured Kr_2F emission intensity during deposition (up to the dip in the spectra) and for prolonged irradiation. The spacer layers are 5.6 (curve 1) and 1.1 (curve 2) nm thick. The assumed penetration depth $d_0 = 1.3$, 2.5 and 5 nm for the modeled curves are indicated. For a detailed discussion of the model the reader is referred to Ref. 21.

It is important, however, that now a check of consistency for each sample is possible between the rise according to Fig. 9 and the attenuation by the pure Ar spacer according to Fig. 8. In this way a reliable $d_0 = 2.1$ nm corresponding to 8 or 9 monolayers was established [21]. This value is close to the earlier results and consistent with the discussion in terms of s_0 and l . In addition, it was found that several samples yield a significant penetration probability for rather large spacer thickness on the order of 10 nm. The effect was attributed to multiple excitation of the F atoms induced by impurities. Prolonged irradiation allows to cross large thicknesses by this unintentional multistep excitation. The effect has to be kept in mind as a source for an overestimate of d_0 in related experiments.

3.3. Multiply doped films and crystals

This subject has been reviewed recently [1] and some main results are summarized briefly. The realization of high gain solid state excimer laser was based on the formation of a high density of XeF in Kr, Ar, and Ne matrices [22,23]. The XeF centers are prepared by F₂ dissociation and transport of the F fragments to the Xe dopants. It was immediately recognized that the F atoms undergo long-range migration [24]. A systematic study of the migration properties was carried out by shuttling F atoms between Xe and Kr dopants in an Ar crystal [25]. The kinetic energy of the F atoms of ~ 0.5 eV was acquired by emission of the KrF and XeF exciplexes to the repulsive ground state. An average length of travel of 5 to 8 nm or 10–15 lattice constants was derived from the shuttling kinetics assuming a statistical distribution of the dopants. The bimolecular recombination of F atoms in Ar crystals was recorded via the bleaching of the Ar₂⁺F⁻ emission in an analogous study and an average length of travel of 7 nm was obtained for an estimated kinetic energy of 0.7 eV [26]. For Kr crystals co-doped with F₂ and Xe it was observed that the F atoms migrate an average length of (8 ± 4) nm for a kinetic energy of 2.4 eV, while they remain localized below 1.9 eV [27].

The high mobility of F atoms was exploited quite early to establish new photochemical reactions in matrices [7,28,29]. This field is very active and a major improvement represents the combination of ESR and IR analysis with optical spectroscopy [30–33]. A quantitative study of the migration lengths used the kinetics in the addition reactions of F to CO and O₂ [34]. The comparison of vapor-deposited matrices with results from free standing crystals shows a dramatic increase from 0.7–1.4 nm in the films to (14 ± 6) nm in the crystals. The influence of the morphology on the observed migration length has to be

strongly emphasized. There is a long-standing experience on the art of sample preparation. Especially the condensation of films has to be carried out with an optimization of condensation temperature and rate to avoid porous or disordered structures [1]. Therefore the preparation and structure of the films studied in Sec. 3.1 and 3.2 was carefully controlled. In summary the results from the multiply doped samples emphasize a considerable average length of travel of neutral F atoms typically of the order of 5 to 10 nm for samples with good structural quality. The results are compatible with those from Sec. 3.2, since the penetration depth d_0 yields a lower bound for the average length of travel s_0 and estimates for s_0 fall into this range. Some of the values for small kinetic energies in multiply doped samples appear to be rather close to the upper limit. The method of multiple doping has to deal with the statistical averaging and with a possible deformation of the lattice in the vicinity of the dopants. This was a motivation to investigate sandwich structures with a transport through the pure spacer layer. It is quite satisfying that both methods yield consistent and quite large average length of travel.

4. Femtosecond pump-probe spectroscopy

Femtochemistry allows to follow the intermediates in a photochemical reaction on a molecular timescale [35]. The method is therefore well suited to study the recombination dynamics in the matrix cage as well as cage exit and presumably migration. ClF molecules were established as a good source to follow the dynamics of F atoms in matrices [36]. Emission from the bound A' state of ClF to the ground state allows to record the remaining concentration of ClF molecules. The quantum yield for permanent dissociation of ClF in Ar, i.e., cage-exit of the F fragment without geminate or non-geminate recombination, was measured to be 5 %. In Kr matrices the decay of ClF concentration is an order of magnitude faster.

A prerequisite is, that the sample composition is approximately constant over the whole pump-probe scan. In the case of ClF in Ar, the dissociation efficiency is sufficiently small. In Kr matrices, the fluorescence from the excimer states Kr⁺F⁻ leads to a mobilization of the F fragments and can be used to prepare a convenient equilibrium [37] in the reaction ClF+Kr \rightleftharpoons Cl+KrF. The femtosecond experiments are carried out in this equilibrium which slowly decays because F atoms are expelled from the laser focus by sequential reexcitation. The F fragments accumulate in a ring around the laser focus. This can be verified by translating the sample perpendicularly to the laser beam (focal diameter of 100 μ m) after several minutes of irradiation. While the Kr⁺F⁻ fluorescence

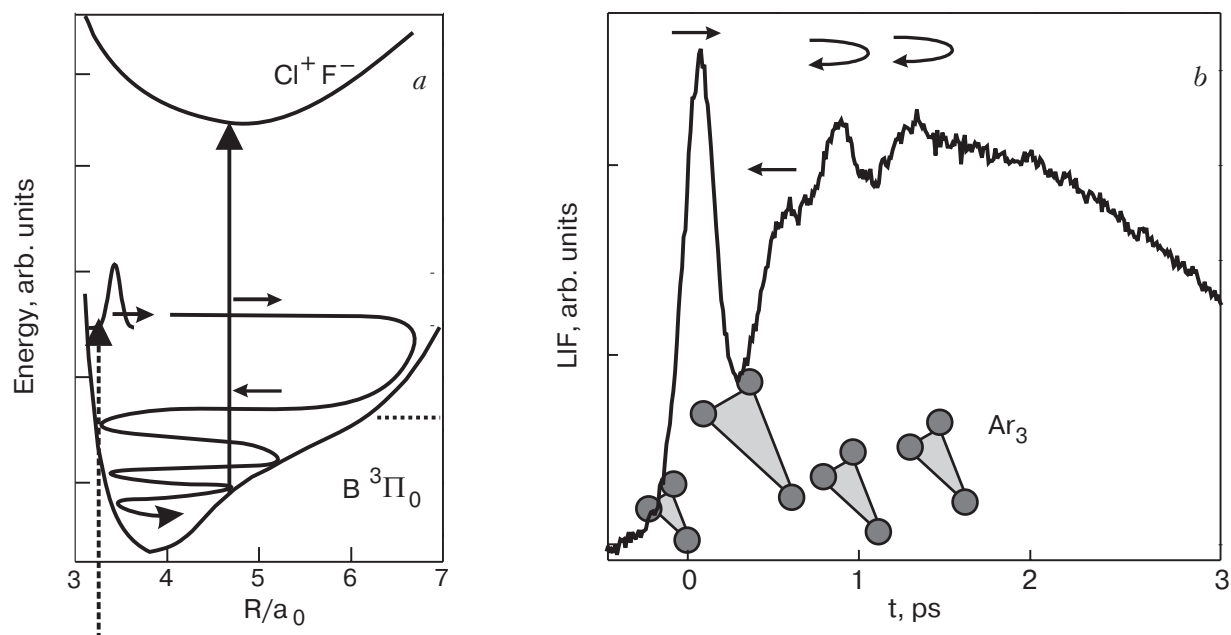


Fig. 10. *a*) Scheme of the wave packet dynamics with the probe window indicated by the vertical arrow at $R_{\text{win}} = 4.8 a_0$ that yields the pump-probe spectrum in panel *b*. The wave packet is excited (dashed vertical arrow) above the gas phase dissociation limit (dotted line) and loses energy in the *B*-state due to interaction with the cage. *b*) fs-pump-probe spectrum with $\lambda_{\text{pump}} = 387 \text{ nm}$ and $\lambda_{\text{probe}} = 319 \text{ nm}$. The arrows above the peaks indicate how the wave packet passes through the window. Further discussion of the wave packet dynamics can be found in Ref. 38.

in the original spot has significantly decayed, it increases when the ring around this focus is probed. Thus the F fragments are transported over this macroscopic length scale by successive reexcitation. A detailed description of the equilibrium and F transport will be given elsewhere [10].

To apply the ultrafast spectroscopy, both the pump and the probe transition must lie in a spectral range which is accessible with femtosecond laser sources. The dynamics of the ClF molecule itself can be conveniently followed by probing to the Cl^+F^- manifold with $\lambda_{\text{probe}} < 320 \text{ nm}$. The dissociated F fragments can be monitored by exciting the Kr^+F^- excimer with an ultrafast pulse at $\lambda_{\text{probe}} < 270 \text{ nm}$ [37]. The formation of Ar^+F^- from F fragments in Ar requires much shorter wavelengths ($\lambda \sim 210 \text{ nm}$) which are at present not easily accessible with femtosecond lasers. This problem can be circumvented by co-doping the Ar matrix with Kr or Xe.

The recombination dynamics of ClF — as opposed to cage exit — is studied by preparing a vibrational wave packet near the inner turning point on the repulsive limb of the *B* state with a short laser pulse according to the scheme in Fig. 10,*a*. The passage of the wave packet through the spatial region of a delayed probe pulse leads to an excitation to the ionic ClF states. The intensity of the emission from the ionic states versus the time delay thus monitors the time sequence of passages through the probe window. The

measured time course [38] in Fig. 10,*b* displays the outward motion of the wave packet (\rightarrow) the return from the outer turning point (\leftarrow) and the following oscillations (\leftrightarrow). The analysis of the spectrum shows that the wave packet loses most of its kinetic energy during the long lasting outer bow in the first collision with the cage [38] in accord with the simulation [15]. The recombining wave packet does not reach out so far due to the energy loss and in the next passages it is caught near the outer turning point. The wave packet can be scattered with skewed angles from the matrix cage. If an aligned ensemble of excited ClF molecules is prepared by photoselection with a polarized pump beam, probing the polarization dynamics shows that the bond direction is tilted within few oscillations on a timescale of 1.2 ps [39]. This ultrafast reorientation by scattering and recombination has to be well distinguished from a usual rotation which even in the free molecule would lie in the 100 ps range. The dynamics of nonradiative transitions between electronic states was investigated via the spin flip from a repulsive singlet state to bound triplet states. This nonradiative transitions are surprisingly fast and 40 % to 50 % of the final triplet population is reached already after the wave packet returns from its first encounter with the cage, i.e. in about 500 fs [40]. This result agrees very well with the simulations [15].

First results on cage exit and localization of the wave packet in a neighboring cage are presented in the

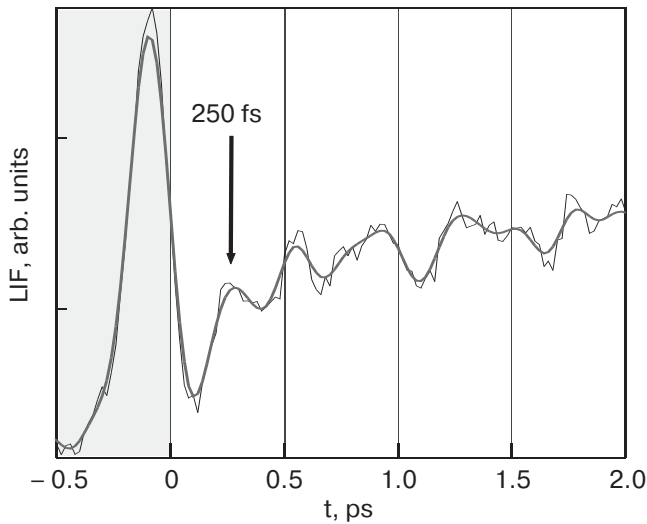


Fig. 11. Normalized Kr_2F fluorescence intensity for ClF/Kr (1/1000) at $T = 5$ K as a function of the time delay t between two fs pulses at $\lambda_1 = 387$ nm and $\lambda_2 = 270$ nm. The process that leads to the formation of the Kr_2^+F^- excimer is indicated in Fig. 12,a for positive time delays and in Fig. 12,c for negative time delay t . For $t > 0$ the fs-pump-probe spectrum measures the ultrafast direct cage exit of F in Kr. After $t = 250$ fs the first F atoms have reached the nearest interstitial site.

following, however, a detailed description will be given elsewhere [10]. ClF in Kr is excited with a sequence of two fs-pulses with a duration of approx. 100 fs at the wavelengths $\lambda_1 = 387$ nm and $\lambda_2 = 270$ nm. The fluorescence from the Kr_2^+F^- excimer (lifetime ~ 150 ns) is recorded as a function of the time delay between the two fs-pulses. The 270 nm pulse probes all F atoms that have been accumulated in the course of the experiment. To detect a fs-pump-probe signal of the hot escaping F atoms, it is necessary to employ a differential technique that subtracts the strong background from these accumulated F atoms. Figure 11 shows the resulting Kr_2^+F^- fluorescence as a function of time delay between the pulses at λ_1 and λ_2 . Care is taken to accurately determine the time zero when the two pulses overlap «in situ» by a FROG-cross correlation [41]. The interpretation of the spectrum for positive time delays $t > 0$ is straight forward. The pump pulse $\lambda_1 = 387$ nm excites ClF to its bound $^3\Pi$ state beyond the dissociation limit (cf. Fig. 12,a). After approximately 250 fs, a first maximum in the signal indicates that the F atoms have arrived in the nearest interstitial site (O_h). Here $\lambda_2 = 270$ nm excites the «hot» KrF to Kr^+F^- which leads to the Kr_2^+F^- configuration and emission after structural rearrangement. This time agrees very well with the prediction for direct cage exit from the simulations [15] and corresponds to a straight flight of the F atom through the triangular window of Kr atoms as

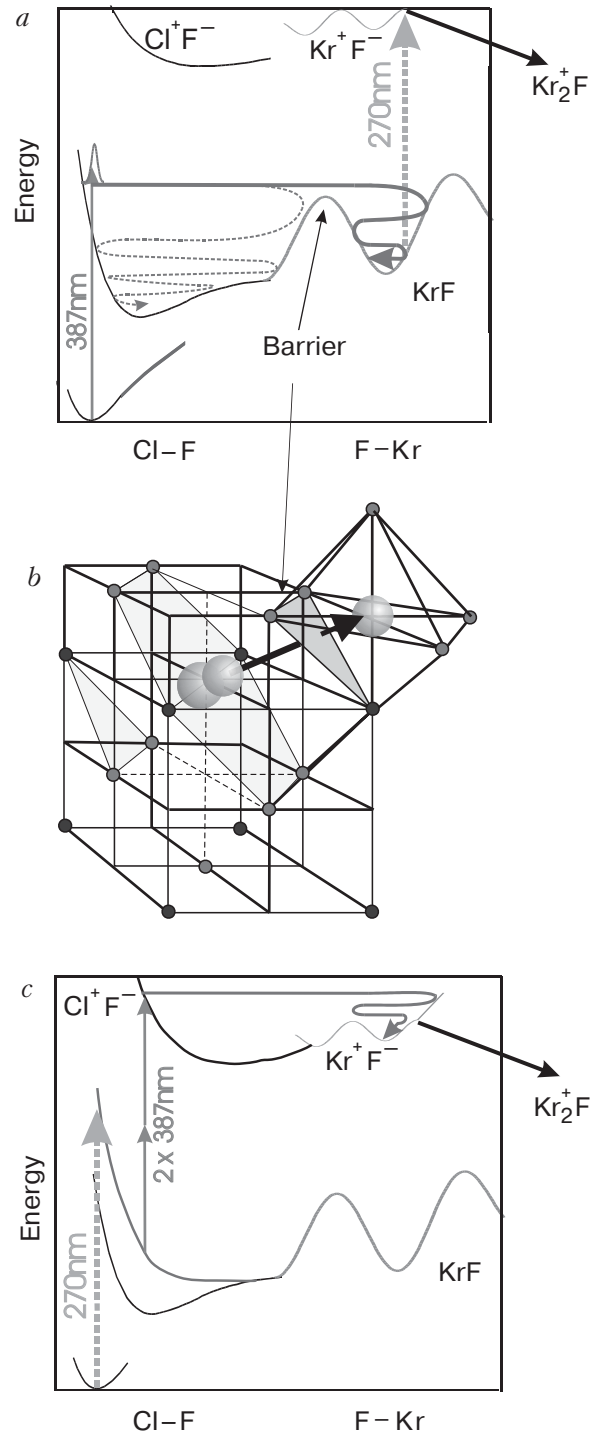


Fig. 12. a) Scheme for the pump-probe spectrum in Fig. 11 for $t > 0$. The pump-pulse $\lambda_1 = 387$ nm prepares a wave packet on the bound $^3\Pi$ state of ClF . The F atom leaves the cage, overcoming the barrier and can be probed by $\lambda_2 = 270$ nm to form the Kr^+F^- excimer. b) ClF molecule on a single substitutional site of the Kr fcc lattice. The arrow indicates the direction of the F atom's cage exit. c) Scheme explaining the peak at $t = -50$ fs in Fig. 11. $\lambda_2 = 270$ nm prepares a wave packet on the repulsive $^1\Pi$ state of ClF . A two photon resonance after 50 fs transfers the wave packet to the ionic Cl^+F^- manifold. F^- exit, rearrangement and relaxation lead to the Kr_2^+F^- excimer.

indicated by the solid arrow in Fig. 12,*b*. The signal keeps rising in the first 2 ps and is essentially constant for 100 ps. The assignment of the structures after the first peak requires further experimental and theoretical effort, since they originate from both delayed cage exit and migration of the F fragments within the matrix. For positive time delays the signal is linearly dependent on the intensity of both pulses, in accord with the scheme in Fig. 12,*a*.

For negative time delays, the $\lambda_2 = 270$ nm pulse takes the role of the pump pulse and a two-photon transition with $\lambda_1 = 387$ nm is used as a probe. The peak at $t = -50$ fs depends quadratically on the intensity of the $\lambda_2 = 387$ nm probe pulse. Figure 12,*c* shows the corresponding pump-probe scheme. The pulse at $\lambda_2 = 270$ nm excites ClF to its repulsive $^1\Pi$ state. After 50 fs, while the Cl-F is stretching on the $^1\Pi$ surface, an efficient two-photon transition at $\lambda_2 = 387$ nm transfers the wave packet to the ion-pair manifold Cl^+F^- . This is consistent with the potential energy diagram of ClF [42] and with the fact that only one peak is observed at negative time delays, since vibrational and nonadiabatic decay to $^3\Pi$ prohibit another excitation when the wave packet returns. After absorption of λ_1 and λ_2 in this time ordering, the wave packet travels towards larger Cl^+F^- distances on the ionic manifold (Fig. 12,*c*). The F^- ion may reach a nearest neighbor cage as indicated in Fig. 12,*b* by the solid arrow and show the same fluorescence from Kr_2^+F^- after relaxation within the excimer state. The experiment demonstrates that the F^- ion can overcome the barrier for cage exit within the ionic manifold, however, the pump-probe delay contains no information on the dynamics of the cage exit of the F^- ion, as the time between pump and probe pulse is spent on the valence states. Here it may be more appropriate to call λ_1 the pump pulse and λ_2 the control pulse, which determines the yield for F^- cage exit.

5. Conclusion

Fluorine ions have rather small penetration depths (Sec. 3.1). The transmission of F^+ through Kr and Xe films is near zero for one monolayer. The damping to a transmission of $1/e$ which is used throughout the paper for the definition of penetration depth and average length of travel occurs already for a half monolayer.

The experimental evidence for neutral F atoms, in contrast, yields much larger penetration depths. The early studies of multiply doped Ar crystals are described by a reaction cross sections with other particles on the track of the mobile F atom (Sec. 3.3). Therefore the derived track length corresponds to the number of visited sites and is correlated with the aver-

age length of travel s_0 . Considerations on multiply visited sites etc. were not included in the evaluation of the kinetics. These measurements, carried out by several groups for various reaction partners, consistently yield an average length of travel on the order of $s_0 = 7$ to 10 nm in well ordered Ar samples. It was shown that the average length of travel may be reduced to 1 nm in disordered matrices. The interpretation of the multiple-doping experiments could be questioned concerning the assumed statistical distribution of dopands and a modification of the F mobility by lattice deformations in the vicinity of the dopands. In addition, the kinetic energy was provided by a rather intense laser excitation that dissociates F_2 molecules, and the locally deposited energy could mobilize previously generated F atoms that are trapped in the vicinity. This unintentional reexcitation can enlarge the observed length of travel.

Therefore, the penetration depth d_0 of F atoms through an Ar film of well defined thickness was determined in the sandwich experiments (Sec. 3.2). In this way the excitation region is separated from the transport region, the transport region is spatially well defined and lattice distortions by dopands are avoided. In carefully prepared and characterized Ar films, a penetration depth around 2 to 3 nm was observed in several independent measurements. Multiple excitations were excluded according to the spectroscopy. This assumption and the consistency of the data were checked by monitoring the penetration kinetics during growth of the top layer, which delivers the F atoms by F_2 dissociation. Slowing down the deposition rate in such a way that most of the F_2 molecules are dissociated on the actual surface before it is covered by the next monolayer allows to decide, whether F atoms are remobilized after completion of the film. In several samples remobilization indeed occurred and was attributed to unintentional impurities. Sorting out the well behaving samples resulted once more in a penetration depth between 2 and 2.5 nm.

To compare the penetration depth d_0 with the average length of travel s_0 from the multiply doped samples, the different geometries have to be taken into account. The penetration depth d_0 corresponds to a vertical and straight path through the spacer layer. The isotropic angular distribution of the initial momentum of the F atoms leads to a corresponding average length of travel s_0 significantly larger than the measured d_0 , even for straight trajectories. A diffusive type of motion enlarges s_0 furthermore and a realistic estimate of $s_0 = 7$ nm was derived from the d_0 values. This is on the lower limit of the range derived from the multiple doping experiment and consistent within the error bars. Thus the experiments show that F atoms

provided with several eV of kinetic energy travel more than 2 nm in Ar matrices, i.e. at least 8 monolayers.

If we contrast the experimental findings with the calculations (Sec. 2), we arrive at a severe discrepancy. The very first molecular dynamics simulations looked promising and predicted long range trajectories which exceed the chosen size of the cluster. Advanced calculations, which treat the interaction of the F atom's p -orbital with the matrix in more detail and include nonadiabatic transitions among the electronic surfaces, yield much shorter travel ranges. Improvements of the potentials by using the DIM method did not resolve the problem. All more recent high level calculations predict cage exit only to neighboring sites and no long range mobility at all.

On the other hand, these simulations deliver a swarm of trajectories on the femtosecond timescale. The recombination dynamics of ClF molecules in Ar, studied in a first set of femtosecond pump-probe experiments, agrees well with the predictions of the DIM-trajectory simulations on F₂ as far as the very fast energy loss and the redistribution in the manifold of electronic states are concerned (Sec. 4). Finally, the cage exit dynamics of the F fragment, measured in ClF doped Kr samples, shows a time for direct cage exit to the next site within 250 fs, in good agreement with the predictions. It seems that the discrepancies between experiment and high level simulations are on a rather subtle level, that allows for a convincing prediction of the short time-dynamics (up to 1 ps) but precludes correct simulation of the migration.

Thus it is up to a monitoring of the migration process itself by femtosecond spectroscopy to pin down where the demonstrated deviation between experiment and simulations occurs. This may be accomplished, e.g., by combining the femtosecond spectroscopy with co-doped matrices.

Acknowledgment

This collection of results was obtained in long-standing collaborations with the groups of Prof. V.A. Apkarian, Prof. B. Gerber, Prof. J. Manz, and Prof. H. Gabriel.

1. V.A. Apkarian and N. Schwentner, *Chem. Rev.* **99**, 1481 (1999).
2. R. Alimi, R.B. Gerber, and V.A. Apkarian, *J. Chem. Phys.* **92**, 3551 (1990).
3. V. Biryukov, *Nucl. Instrum. Methods Phys. Res.* **B53**, 202 (1991).
4. N. Sack, M. Akbulut, T. Madey, P. Klein, H. Urbassek, and M. Vicanek, *Phys. Rev.* **B54**, 5130 (1996).
5. C. Bressler and N. Schwentner, *Phys. Rev. Lett.* **76**, 648 (1996).
6. E. Misochko, A. Akimov, and C. Wight, *Chem. Phys. Lett.* **274**, 23 (1997).
7. C. Bressler, W. Lawrence, and N. Schwentner, *J. Chem. Phys.* **105**, 1318 (1996).
8. G. Zerza, G. Sliwinski, and N. Schwentner, *Appl. Phys.* **B55**, 331 (1992).
9. G. Zerza, F. Knopp, R. Kometer, G. Sliwinski, and N. Schwentner, *UV-VIS Solid State Excimer Laser - XeF in Crystalline Argon*, in: *Solid State Laser II*, *SPIE* **1410**, 202 (1991).
10. M. Bargheer and N. Schwentner, in preparation.
11. R. Alimi, R.B. Gerber, and V.A. Apkarian, *Phys. Rev. Lett.* **66**, 1295 (1991).
12. A. Krylov and R. Gerber, *Chem. Phys. Lett.* **231**, 395 (1994).
13. A. Krylov, R. Gerber, and V. Apkarian, *Chem. Phys.* **189**, 261 (1994).
14. K.S. Kizer and V.A. Apkarian, *J. Chem. Phys.* **103**, 4945 (1995).
15. M.Y. Niv, M. Bargheer, and R.B. Gerber, *J. Chem. Phys.* **113**, 6660 (2000).
16. M. Ovchinnikov and V.A. Apkarian, *J. Chem. Phys.* **110**, 9842 (1999).
17. M. Akbulut, N. Sack, and T. Madey, *Surf. Sci. Rep.* **28**, 177 (1997).
18. N. Sack, M. Akbulut, and T. Madey, *Phys. Rev.* **B51**, 4585 (1995).
19. C. Bressler, M. Dickgiesser, and N. Schwentner, *J. Chem. Phys.* **107**, 10268 (1997).
20. M. Dickgiesser and N. Schwentner, *J. Phys. Chem.* **A104**, 3743 (2000).
21. M. Dickgiesser and N. Schwentner, *J. Chem. Phys.* **113**, 8260 (2000).
22. M. Frankowski, G. Sliwinski, and N. Schwentner, *J. Low. Temp. Phys.* **122**, 443 (2001).
23. M. Frankowski, G. Sliwinski, and N. Schwentner, in: *Proceedings, Laser Physics and Applications* **3724**, 362 (1999).
24. N. Schwentner and V. Apkarian, *Chem. Phys. Lett.* **154**, 413 (1989).
25. H. Kunttu, J. Feld, R. Alimi, A. Becker, and V. Apkarian, *J. Chem. Phys.* **92**, 4856 (1990).
26. H.K. J. Feld and V.A. Apkarian, *J. Chem. Phys.* **93**, 1009 (1990).
27. H. Kunttu, E. Sekreta, and V.A. Apkarian, *J. Chem. Phys.* **94**, 7819 (1991).
28. M. Jacox, *Rev. Chem. Interm.* **6**, 77 (1985).
29. R. Perutz, *Chem. Rev.* **85**, 77 (1985).
30. I. Goldschleger, E. Misochko, A. Akimov, and C. Wight, *J. Mol. Spectrosc.* **205**, 269 (2001).
31. E. Misochko, A. Akimov, and C. Wight, *J. Phys. Chem.* **A103**, 7972 (1999).
32. E. Misochko, A. Akimov, I. Goldschleger, and C. Wight, *Fiz. Nizk. Temp.* **26**, 981 (2000) [*Low Temp. Phys.* **26**, 727 (2000)].
33. E. Misochko, A. Akimov, I. Goldschleger, and C. Wight, *J. Chem. Phys.* **116**, 10318 (2002).

34. E. Misochko, A. Akimov, and C. Wight, *Chem. Phys. Lett.* **293**, 547 (1998).
35. A.H. Zewail, *J. Phys. Chem.* **A104**, 5660 (2000).
36. M. Bargheer, P. Dietrich, and N. Schwentner, *J. Chem. Phys.* **115**, 149 (2001).
37. M. Bargheer, *Ultrafast Photodynamics in condensed phase*, Shaker, Aachen (2002), ISBN 3-8322-0814-3.
38. M. Bargheer, J. Pietzner, P. Dietrich, and N. Schwentner, *J. Chem. Phys.* **115**, 9827 (2001).
39. M. Bargheer, M. Gühr, and N. Schwentner, *J. Chem. Phys.* **117**, 5 (2002).
40. M. Bargheer, M.Y. Niv, R.B. Gerber, and N. Schwentner, *Phys. Rev. Lett.* **89**, 108301 (2002).
41. M. Bargheer, K. Donovang, P. Dietrich, and N. Schwentner, *J. Chem. Phys.* **111**, 8556 (1999).
42. A.B. Alekseyev, H. Liebermann, R.J. Buenker, and D.B. Kokh, *J. Chem. Phys.* **112**, 2274 (2000).